Journal of Machine Construction and Maintenance
QUARTERLY ISSN 1232-9312 4/2018(111)
p. 41–46

Grzegorz JÓŹWIAK[a,b,*], Magdalena MOCZAŁA-DUSANOWSKA[b,c], Krzysztof GAJEWSKI[b], Andrzej SIERAKOWSKI[d], Piotr WÓJCICKI[d]

[a] Institute for Sustainable Technologies – National Research Institute, Radom, Poland
[b] Faculty of Microsystems Electronics and Photonics, Wrocław University of Science and Technology, Poland
[c] Physikalisches Institut, Universität Würzburg, Germany
[d] Institute of Electron Technology, Warsaw, Poland
[*] Corresponding author: grzegorz.jozwiak@itee.radom.pl

ESTIMATION OF SHAPE OF AFM TIP WITH "CROSS-FORREST" CALIBRATION STANDARD

Key words: atomic force microscopy, blind tip reconstruction, calibration standard

Abstract: The "Cross-Forrest" tip shape calibration standard for regularized blind tip reconstruction has been fabricated and investigated. The confirmation of previously reported theoretical findings is shown. However, the KSVD-OMP algorithm of images denoising has been extended by additional group sparsity penalty and Shi Tomasi corner detection algorithm with 100 nm size window for cross concave corners needed to be applied. The comparison of SEM direct tip imaging with 3D shapes reconstructed on the basis of filtered and unfiltered AFM images are shown and the qualitative agreement has been confirmed. The optimization of fabrication technology of "Cross-Forrest" structure is required to allow quantitative tip shape measurements. It should limit the uncertainty of the initial shape of an AFM tip, and the resulting uncertainty of final shape which is the improved version of the initial one.

Estymacja kształtu ostrza AFM za pomocą struktury kalibracyjnej „Cross-Forrest"

Słowa kluczowe: mikroskopia sił atomowych, ślepa rekonstrukcja kształtu ostrza, struktura kalibracyjna.

Streszczenie: Wykonano i zbadano strukturę „Cross-Forrest" służącą do kalibracji kształtu ostrza metodą regularyzowanej ślepej rekonstrukcji. Potwierdzono prezentowane w literaturze wyniki teoretyczne. Wymagało to jednak rozszerzenia algorytmu filtracji obrazów KSVD-OMP o dodatkową funkcję kary w postaci wskaźnika grupowej rzadkości reprezentacji oraz zastosowania algorytmu Shi-Tomasiego z 100 nm oknem do detekcji wklęsłych narożników krzyża. Porównano obrazy SEM ostrzy z ich trójwymiarowymi rekonstrukcjami kształtu i potwierdzono zgodność jakościową. Do uzyskania zgodności ilościowej niezbędna jest jednak optymalizacja technologii wykonania struktur „Cross-Forrest", która pozwoli ograniczyć niepewność oszacowania kształtu początkowego ograniczającą niepewność oszacowania kształtu finalnego.

Introduction

Scanning probe microscopy (SPM) is known as a versatile tool for the measurement of properties of nanometre sized objects. Despite its popularity, the quantitative measurements with this technique are still challenging. The most uncertain factor hindering measurements traceability is the shape of the SPM tip.

Many different methods were used to determine the shape of SPM tip and some review can be found in [1]. The problem with tip estimation is caused by the metrological paradox – 3D shapes of nanometre size object are measured by a nanometre size tip which is also a nanometre size object. This fact is taken into account only by the blind tip reconstruction method, which estimates the upper bound on the shape of a tip. That is, it finds the bluntest tip that could be used to obtain the measured image of an unknown surface. Few researchers introduce similar algorithms at the same time [2–4]. Villarubia in [5] presented not only algorithm description but also the source codes in C language which allows his implementation to gain popularity.

The main disadvantage of the BTR algorithm is its sensitivity to noise. Different authors presented some modifications of this procedure to handle this issue [6–10].

The necessity of the optimization of the shape of calibration standard was introduced in [11] and tip shape errors caused by calibration standard were investigated in [12].

Recently, in [13], the influence of advanced filtration techniques on the BTR process was tested. A pocket in the shape of cross was proposed as a calibration standard. It was shown that this shape can be used for BTR and is prone to filtration techniques based on sparse representation of an AFM image. This solution differs from [11,12], because the proposed shape of calibration standard also supports image pre-processing and not only the tip reconstruction. In the proposed structure, wear prone and difficult to fabricate spikes are also avoided.

In the paper, the "Cross-Forrest" calibration standard based on results presented in [13] is shown. The non-perfect shape of a calibration standard enforced some modifications of algorithms presented in [13]. They are described in the following section.

1. Methodology

The "Cross-Forrest" calibration standard was fabricated in ITE Warsaw. The surface of (100) silicon wafer was oxidized to get a 100 nm thick SiO_2 layer. Using photolithography and plasma etching, the structures paths and navigation marks were fabricated. The "crosses" were defined by electron beam lithography and made by deep reactive ion etching (DRIE). Afterwards, the SiO_2 layer was removed by wet etching.

In Figure 1 the scanning electron microscopy (SEM) images of the "Cross-Forrest" standard are shown. The whole structure is a 92 μm x 92 μm square area covered by crosses (Fig. 1a). The shape of a cross is presented in Figure 1b. The cross size is about 1 μm (980 nm in Fig. 1b) and the width of arms changes from 300 nm to 400 nm. The structure's depth ranges from 800 nm to 900 nm.

The AFM images of proposed calibration sample were analysed using the RBTR algorithm [9]. The procedure of the estimation of initial tip shape was modified, since the calibration standard is generally spikes free. Moreover, the filtration algorithm reported in [13] was used to denoise images of a calibration standard. An additional penalty term was applied to KSVD dictionary learning algorithm to ensure similar representation for the same image patches. The filtration algorithm based on dictionary learned from image patches is presented. A detailed description of these algorithms is presented in the following subsections.

1.1. Blind tip reconstruction algorithm

The blind tip reconstruction algorithm is a procedure that tries to inverse the morphological grey-scale dilation operation [4]. It can be only accomplished under an additional condition, i.e. the shape of the tip should be as blunt as possible. With this additional criterion, the following iterative procedure should be able to estimate the shape of a tip.

$$P_{i+1} = \bigcap_{\mathbf{x}\in I}\left[\left(I + \mathbf{t_H} - \mathbf{x}\right) \oplus P_i'\left(\mathbf{x}\right)\right] \cap P_i \tag{1}$$

with $P_i'\left(\mathbf{x}\right) = P_i \cap \mathbf{x} - I - \mathbf{t_H}$ and $\mathbf{t_H} = [00t_H]^T$

P is the inversion in the apex point of a tip shape together with the volume below, I is an AFM image of a calibration standard together with the volume below. $P+x$ means the translation of P by vector x, $-I$ is inversion in the origin of coordinate system, t_H is a regularization parameter that controls noise impact.

The initial P_0 shape is estimated on the basis of the intersection of four concave cross corners. They are identified with the help of histogram-based segmentation algorithm and Shi-Tomasi corner detector [14].

The maximum response of Shi-Tomasi detector is selected; and, after that, the response matrix in the 50nm x 50 nm neighbourhood is zeroed. These two steps are repeated 12 times. They reveal 12 corners of the cross. The four corners that are closer to the centre of the image are used to determine initial shape of a tip.

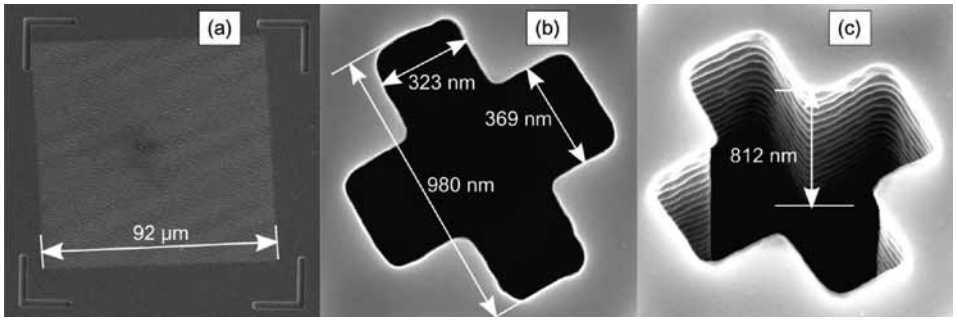

Fig. 1. SEM images of Cross-Forrest calibration standard. (a) top view where navigation marks are visible, (b) zoomed view of a single hole in the shape of cross-horizontal dimensions are shown, (c) perspective view – the depth of hole is presented

1.2. KSVD-OMP filtration algorithm

KSVD-OMP stands for *k* singular value decompositions with orthogonal matching pursuit [15]. The algorithm is an optimization procedure where the following metric is minimized.

$$\left\{\hat{\boldsymbol{\alpha}},\hat{\mathbf{D}},\hat{\mathbf{X}}\right\}=\arg\min_{\boldsymbol{\alpha},\mathbf{D},\mathbf{X}}\left\{\lambda\left\|\mathbf{X}-\mathbf{Y}\right\|_2^2+\sum_{ij}\mu_{ij}\left\|\boldsymbol{\alpha}_{ij}\right\|_0+\right.$$
$$\left.+\sum_{ij}\left\|\mathbf{D}\boldsymbol{\alpha}_{ij}-\mathbf{R}_{ij}\mathbf{X}\right\|_2^2\right\} \quad (2)$$

$\mathbf{Y}$ is an image being denoised, $\hat{\mathbf{X}}$ denoised image, $\hat{\mathbf{D}}$ function dictionary learned from the image, $\hat{\alpha}$ optimal representations of all image patches in the learned dictionary space, and $\mathbf{R}_{ij}$ is a selection matrix composed of zeros and ones used for extraction of patch placed in the image around the point (i,j).

Solving this minimization problem directly would be too complex of a task. Moreover, it is not clear how to determine of optimal values of free parameters λ, μ_{ij}. For this reason, the optimization problem is decomposed. Denoised image $\hat{\mathbf{X}}$ is estimated when the optimal $\hat{\mathbf{D}}$ and $\hat{\alpha}$ are known. So, Equation (2) reduces to the following form:

$$\left\{\hat{\mathbf{X}}\right\}=\arg\min_{\mathbf{X}}\left\{\lambda\left\|\mathbf{X}-\mathbf{Y}\right\|_2^2+\sum_{ij}\left\|\hat{\mathbf{D}}\hat{\alpha}_{ij}-\mathbf{R}_{ij}\mathbf{X}\right\|_2^2\right\} \quad (3)$$

This equation, as it was shown in [13, 15], leads to simple averaging of denoised patches provided that $\lambda = 0$. Patches are denoised by orthogonal matching pursuit algorithm (OMP) [16], which approximately solves the following optimization problem:

$$\hat{\boldsymbol{\alpha}}_{ij}=\arg\min_{\boldsymbol{\alpha}_{ij}}\left\|\boldsymbol{\alpha}_{ij}\right\|_0,\ \textit{provided that}\ \left\|\mathbf{R}_{ij}\mathbf{Y}-\mathbf{D}\alpha_{ij}\right\|_2^2\le\varepsilon \quad (4)$$

This task is realized by the OMP algorithm optimized for batch processing presented in [17].

1.3. KSVD-OMP dictionary learning algorithm with group sparsity penalty function

The last component necessary to solve the problem (2) is the dictionary learning algorithm. To introduce its principle of operation, we assume that the matrix $\mathbf{Z}$ contains N image patches as columns ($\mathbf{z}_n$ is a column vector with elements equal to point values of n-th image patch). Dictionary $\mathbf{D}$ contains S number of function vectors $\mathbf{d}_s$ which are used for sparse approximation of each patch $\mathbf{z}_n$. $\mathbf{A}$ is SxN matrix of representation coefficients (α_{sn} is a coefficient for dictionary function $\mathbf{d}_s$ and patch $\mathbf{z}_n$).

$$\left\{\hat{\mathbf{A}},\hat{\mathbf{D}}\right\}=\arg\min_{\mathbf{A},\mathbf{D}}\left\|\mathbf{A}\right\|_0,\ \textit{provided that}\ \left\|\mathbf{Z}-\mathbf{D}\mathbf{A}\right\|_2^2\le\varepsilon \quad (5)$$

The OMP algorithm is used to find sparse representation for each $\mathbf{z}_n$ patch. After that, the sequential optimization of each dictionary function vector $\mathbf{d}_s$ and the corresponding row vector of nonzero coefficients $\boldsymbol{\alpha}_{s1..N}$ are performed by solving the following rank -1 matrix approximation problem.

$$\left\{\hat{\mathbf{d}}_s,\hat{\boldsymbol{\alpha}}_{s,1..N}\right\}=\arg\min_{\mathbf{e},\mathbf{f}}\left\|\mathbf{Z}_s-\mathbf{D}\mathbf{A}_s+\mathbf{d}_s\boldsymbol{\alpha}_{s1..N}-\mathbf{e}\mathbf{f}\right\|_2^2 \quad (6)$$

$\mathbf{Z}_s$ is a matrix of all image patches having $\mathbf{d}_s$ in their sparse representation, $\mathbf{A}_s$ is a matrix of representation coefficients of patches in $\mathbf{Z}_s$ matrix. This problem can be solved by singular value decomposition (SVD) as presented in the equation below.

$$\mathbf{Z}_s-\mathbf{D}\mathbf{A}_s+\mathbf{d}_s\boldsymbol{\alpha}_{s1..N}=\mathbf{U}\Sigma\mathbf{V}^T,$$
$$\textit{afterwards}\ \ \hat{\mathbf{d}}_s=\mathbf{u}_{1..S1},\hat{\boldsymbol{\alpha}}_{s,1..N}=\sigma_{11}\mathbf{v}_{1..N1}{}^T \quad (7)$$

Since only vectors corresponding to the most significant singular value are necessary to update dictionary function, vector $\mathbf{d}_s$, SVD is computed by a less expensive power approximation algorithm as was shown in [17]. Although $\mathbf{d}_s$ and $\boldsymbol{\alpha}_{s1..N}$ are optimized at the same time, it cannot be guaranteed that the current representation is optimal. For this reason, after optimization of all dictionary function vectors, the OMP is performed once again. The procedure is repeated as long as the convergence is achieved, which is measured by the lack of progress in representation sparsity.

In comparison to procedure presented in [15], the OMP algorithm has been modified. In the previously presented solution, the selection of dictionary elements is based on a correlation to approximated image patch. To obtain the presented results, we extend this correlation to all patches belonging to the same class/group [18]. Then similar patches get a similar set of dictionary function vectors, which is known under the term group sparsity [19]. The grouping is done by k-means clustering algorithm [20].

2. Results

To investigate the performance of tip shape estimation using the "Cross-Forrest" calibration standard, the AFM images obtained with three different tips and two AFM setups were measured – TESP SS sharpened Bruker probe with declared tip radius below 5 nm, HA-NC composite NT-MDT probe with declared tip radius below 10 nm, and magnetic SC-LM 20 Nano&more probe with declared tip radius below 40 nm. In the case of the TESP SS and HA-NC probes, the Veeco Multimode system was used. Veeco Nanoman was used for the SC-LM probe. After AFM scanning, the tips were imaged by SEM.

In Figure 2, the gathered 3D AFM images are shown. It is shown that the shape of registered holes changes when scanned by different tips. The shape of the bottom of holes not being flat suggest that the tip has not reached the bottom during scanning process, which indicates the limited contact as required in [13]. This fact allows the reduction of the complexity of

RBTR algorithm. The corners of the cross are smooth and irregular, which force the application of Shi-Tomasi algorithm with a window size of 100x100 nanometres for the detection of concave corners when the initial tip shape was estimated.

Then, the AFM images were subjected to the following processing pipeline:

1. Surface slope and bowl correction was made using only flat part of the surface.
2. Corners detection and initial tip shape estimation was carried out.
3. 16x16 patches clusterization by k-means algorithm were performed.
4. KSVD-OMP filtration with group penalty were done (patch size 16x16, noise level as a median deviation from the flat image part).
5. The estimations of tip shapes by RBTR on the basis of both filtered and unfiltered images were completed.

Figure 3 presents the estimated 3D tip shapes. Filtered and unfiltered reconstructions are irregular. It is caused by irregularities in the shape of the fabricated

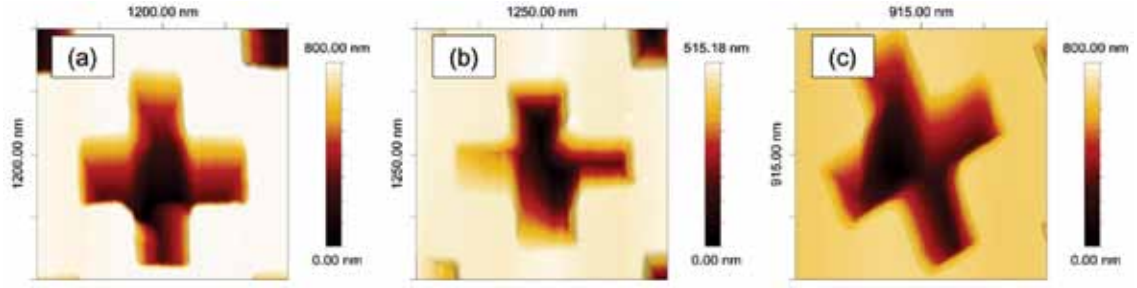

Fig. 2. AFM images of Cross-Forrest calibration standard measure by three different tips: (a) TESP SS probe, (b) HA-NC probe, (c) SC-LM 20 probe

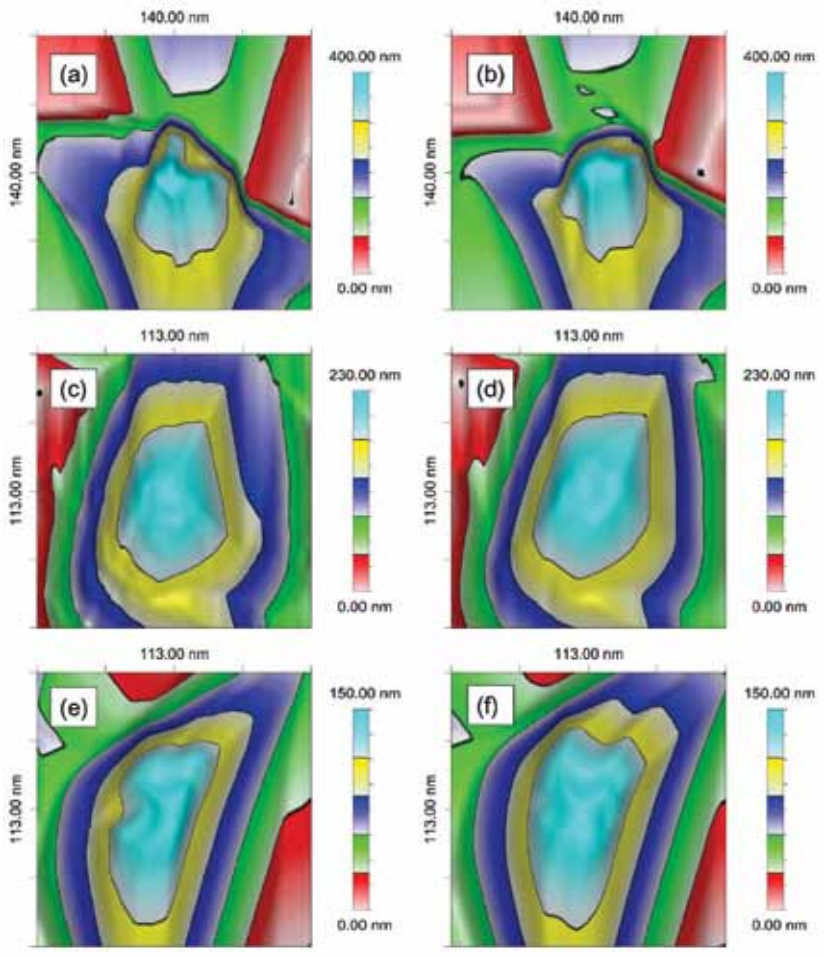

Fig. 3. 3D reconstructions of shapes of tips used to scan images from Figure 2. Reconstructions have been done for unfiltered (left hand side) and filtered images (right hand side): (a,b) TESP SS probe, (c,d) HA-NC probe, (e,f) SC-LM probe

calibration standard. Moreover, the impact of imprecise corner detection is seen in Figures 3a and b, which is also the consequence of irregular concave corners of the calibration standard.

In Figure 4, the orthogonal projections of estimated shapes are shown on the tip's SEM images as a background. The projections of filtered images are smoother and better follow SEM tip profiles, especially close to the tip apex.

Conclusion

In the paper, the results of regularized blind tip reconstruction on the basis of AFM images of "Cross-Forrest" calibration standard are presented. Thanks to the unique shape of this standard RBTR run using only cross edges, which strongly limits computational complexity with minimum information loss, the impact of KSVD-OMP filtration algorithms is shown.

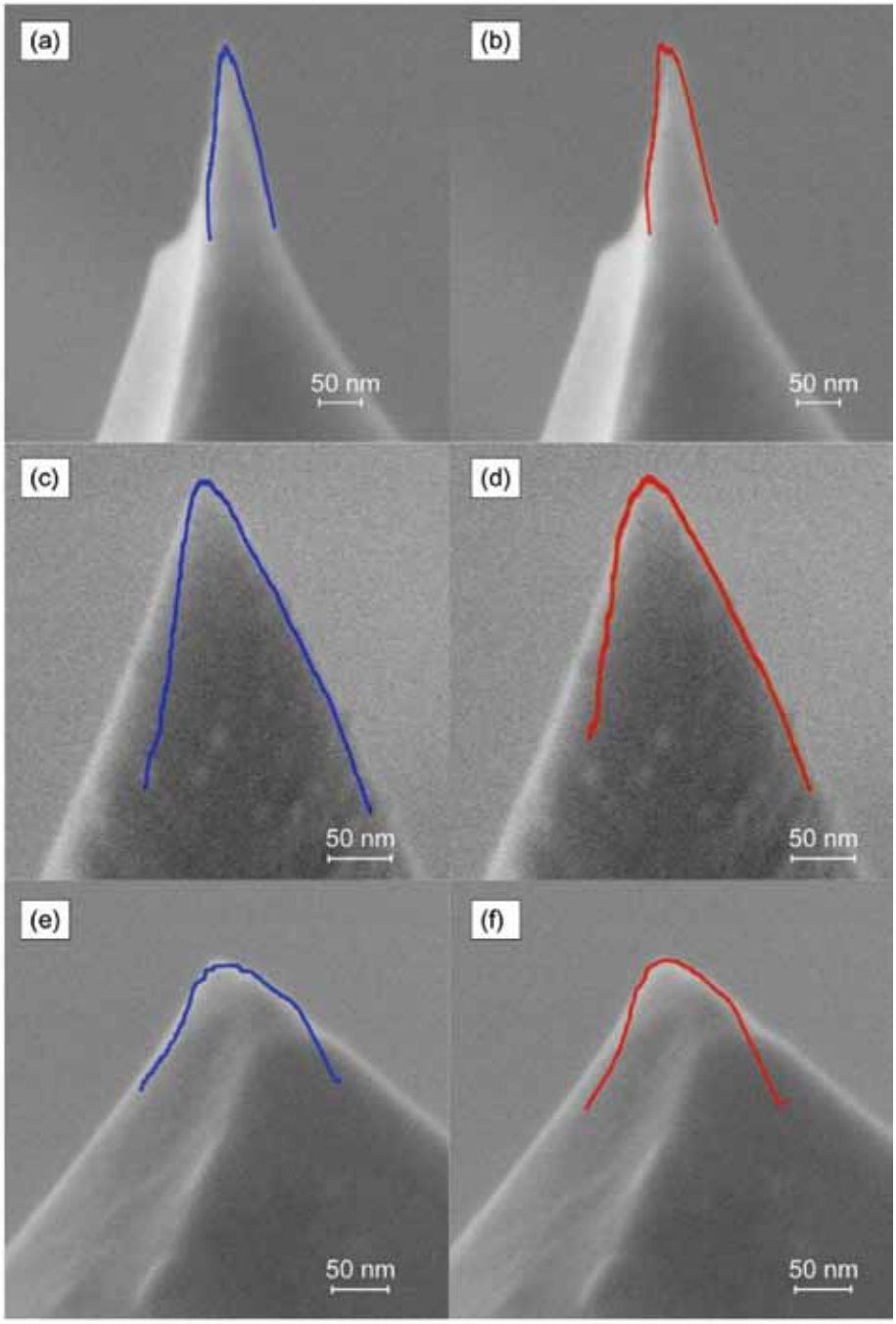

Fig. 4. SEM images of investigated tips with orthogonal projections of reconstructed shapes. Projections have been calculated for shapes reconstructed from unfiltered images (blue lines) as well as from filtered images (red lines). (a,b) TESP SS probe, (c,d) HA-NC probe, (e,f) SC-LM probe

Qualitative agreement between orthogonal projections of 3D shapes of reconstructed tips and their SEM images is shown. The optimization of the technology of fabrication of "Cross-Forrest" standard is required, especially the time of the Bosch cycle in the DRIE process. It should improve the quality of the estimation of initial probe shape and, in consequence, the results of BTR. Unfortunately, the uncertainty of estimated tip shape remains an open problem. Neither of the implementations of BTR algorithm provides uncertainty estimation. However, an optimized "Cross-Forrest" calibration standard with good initial tip estimation could limit this uncertainty to the uncertainty of initial tip; since the RBTR algorithm can only improve the initial shape never worsen.

Acknowledgements

The research was supported by Polish Ministry of Science and Higher Education under program IUVENTUS Plus, grant no. IP2012 017272.

References

1. Danzebrink H.U., Koenders L., Wilkening G., Yacoot A., Kunzmann H.: Advances in Scanning Force Microscopy for Dimensional Metrology. *CIRP Annals – Manufacturing Technology*, 2006, 55(2), pp. 841–878.
2. Dongmo S., Troyon S., Vautrot M., Delain P., Bonnet E.: Blind restoration methods of scanning tunneling and atomic force microscopy images. *Journal of Vacuum Science & Technology B*, 1996, 14, pp. 1552–1556.
3. Williams P.M., Shakesheff K.M., Davies M.C., Jackson D.E., Roberts C.J., Tendler S.J.B.: Blind reconstruction of scanning probe image data. *Journal of Vacuum Science & Technology B*, 1996, 14(2), pp. 1557–1562.
4. Villarubia J.S.: Morphological estimation of tip geometry for scanned probe microscopy. *Surface Science*, 1994, 321(3), pp. 287–300.
5. Villarubia J.S.: Algorithms for scanned probe microscope image simulation, surface reconstruction, and tip estimation. *Journal of Research of the National Institute of Standards and Technology,* 1997, 102(4), pp. 425–454.
6. Williams P.M., Davies M.C., Roberts C.J., Tendler S.J.B.: Noise-compliant tip-shape derivation. *Applied Physics A*, 1998, 66, pp. S911–S914.
7. Todd B.A., Eppell S.J.: A method to improve the quantitative analysis of SFM images at the nanoscale. *Surface Science*, 2001, 491, pp. 473–483.
8. Tian F., Qian X., Villarrubia J.S.: Blind estimation of general tip shape in AFM imaging. *Ultramicroscopy*, 2008, 109, pp. 44–53.
9. Jóźwiak G., Henrykowski A., Masalska A., Gotszalk T.: Regularization mechanism in blind tip reconstruction procedure. *Ultramicroscopy*, 2012, 118, pp. 1–10.
10. Flater E.E., Zacharakis-Jutz G.E., Dumba B.G., White I.A., Clifford C.A.: Towards easy and reliable AFM tip shape determination using blind tip reconstruction. *Ultramicroscopy*, 2014, 146, pp. 130–143.
11. Xu L., Ding Y., Guo Y., Wan J., Wu S., Hu X.: Optimal samples for precision blind tip reconstruction. In: *AOPC 2015: Micro/Nano Optical Manufacturing Technologies; and Laser Processing and Rapid Prototyping Techniques, 2015, Beijing, China*. Proceedings of SPIE, 2015, 9673, 96730I.
12. Wan I., Xu L., Wu S., Hu X.: Investigation on Blind Tip Reconstruction Errors Caused by Sample Features. *Sensors*, 2014, 14(12), pp. 23159–23175.
13. Jóźwiak G.: Noise reduction by sparse representation in learned dictionaries for application to blind tip reconstruction problem. *Measurement Science and Technology*, 2017, 28(3), pp. 034008.
14. Shi J., Tomasi C.: Good Features to Track. In: *Conference on Computer Vision and Pattern Recognition, Seattle (USA), 21–23 June 1994*. IEEE, 1994, pp. 593–600.
15. Aharon M., Elad M., Bruckstein A.: K-SVD: an algorithm for designing overcomplete dictionaries for sparse representation. *IEEE Transactions on Signal Processing*, 2006, 54(11), pp. 4311–4322.
16. Pati Y.C., Rezaiifar R., Krishnaprasad P.S.: Orthogonal matching pursuit: recursive function approximation with applications to wavelet decomposition. In: *27th Asilomar Conference on Signals, Systems and Computers, Pacific Grove (USA), 1–3 Nov. 1993*. *IEEE*, 1993, 1, pp. 40–44.
17. Rubinstein R., Zibulevsky M., Elad M.: 2008 *Efficient Implementation of the K-SVD Algorithm using Batch Orthogonal Matching Pursuit*. [Online]. Technion-Computer Science Department – Technical Report, 2008. [Accessed 3 December 2018]. Available from: www.cs.technion.ac.il/~ronrubin/Publications/KSVD-OMP-v2.pdf
18. Tropp J.A.: Algorithms for simultaneous sparse approximation. *Signal Processing*, 2006, 86, pp. 572–602.
19. Mairal J., Bach F., Ponce J., Sapiro G., Zisserman A.: Non-local sparse models for image restoration. In: *12th International Conference on Computer Vision, Kyoto (Japan), 29 Sept.–2 Oct. 2009*. IEEE, 2009, 11367883.
20. David A., Vassilvitskii S.: K-means++: The Advantages of Careful Seeding. In: *18th annual ACM-SIAM symposium on Discrete algorithms (SODA), New Orleans, Louisiana, 2007*. Proceedings, 2007, pp. 1027–1035.